PORTLAND PRESS

BIOCHEMICAL JOURNAL
ACCEPTED MANUSCRIPT

The different catalytic roles of the metal binding ligands in human 4-hydroxyphenylpyruvate dioxygenase

Chih-Wei Huang, Hsiu-Chen Liu, Chia-Pei Shen, Yi-Tong Chen, Sung-Jai Lee, Matthew D. Lloyd, and Hwei-Jen Lee

4-Hydroxylphenylpyruvate dioxygenase (HPPD) is a non-haem iron(II)-dependent oxygenase that catalyzes the conversion of 4-hydroxylphenylpyruvate (HPP) to homogentisate (HG). In the active site, a strictly conserved 2-His-1-Glu facial triad coordinates the iron ready for catalysis. Substitution of these residues resulted in about a 10-fold decrease in the metal binding affinity, as measured by isothermal titration calorimetry, and a large reduction in enzyme catalytic efficiencies. This study revealed the vital role of the ligand E349 in enzyme function. Substitution of this residue by alanine resulted in loss of activity. The E349G variant retained 5% activity for the coupled reaction, suggesting that coordinating water may be able to support activation of the *trans* bound dioxygen upon substrate binding. The reaction catalyzed by the H183A variant was fully uncoupled. H183A variant catalytic activity resulted in protein cleavage between Ile^{267} Ala^{268} and the production of an N-terminal fragment. The H266A variant was able to produce 4-hydroxyphenylacetate (HPA), demonstrating that decarboxylation had occurred but that there was no subsequent product formation. Structural modeling of the variant enzyme with bound dioxygen revealed the rearrangement of the coordination environment and the dynamic behaviour of bound dioxygen in the H266A and H183A variants, respectively. These models suggest that the residues regulate the geometry of the reactive oxygen intermediate during the oxidation reaction. The mutagenesis and structural simulation studies demonstrate the critical and unique role of each ligand in the function of HPPD, and which correlates with their respective coordination position.

Cite as Biochemical Journal (2016) DOI: 10.1042/BCJ20160146

The different catalytic roles of the metal binding ligands in human 4-hydroxyphenylpyruvate dioxygenase

Chih-Wei Huang[‡§], Hsiu-Chen Liu[†], Chia-Pei Shen[†], Yi-Tong Chen[†], Sung-Jai Lee[†], Matthew D. Lloyd[‖], and Hwei-Jen Lee[†*]

[†]Department of Biochemistry, National Defense Medical Center, Taipei, Taiwan
[‡]Pharmacy Division, Kaohsiung Armed Forces General Hospital, Kaohsiung, Taiwan
[§]Graduate Institute of Medical Sciences, National Defense Medical Center, Taipei, Taiwan
[‖]Medicinal Chemistry, Department of Pharmacy & Pharmacology, Claverton Down, University of Bath, U.K.

Running title: Iron binding ligands of 4-hydroxyphenylpyruvate dioxygenase.

Key words: non-haem Fe(II)-dependent oxygenase; 4-hydroxyphenylpyruvate dioxygenase; iron binding ligands; 2-His-1-carboxylate facial triad; metal binding motif.

[*]To whom correspondence should be addressed. Department of Biochemistry, National Defense Medical Center, No. 161, Sec. 6, Minchuan East Rd., Neihu, Taipei, Taiwan. Tel: +886-2-87910832; Fax: +886-2-87923106; E-mail: hjlee@mail.ndmctsgh.edu.tw

Abbreviations: HPPD, 4-hydroxyphenylpyruvate dioxygenase; HPP, 4-hydroxyphenylpyruvate; HG, homogentisate; HPA, 4-hydroxyphenylacetate; 2-OG, 2-oxoglutarate; HMS, hydroxymandelate synthase; HMA, 4-hydroxymandelate; ITC, isothermal titration calorimetry; QM/MM; Quantum Mechanics/Molecular Mechanics

Abstract

4-Hydroxylphenylpyruvate dioxygenase (HPPD) is a non-haem iron(II)-dependent oxygenase that catalyzes the conversion of 4-hydroxylphenylpyruvate (HPP) to homogentisate (HG). In the active site, a strictly conserved 2-His-1-Glu facial triad coordinates the iron ready for catalysis. Substitution of these residues resulted in about a 10-fold decrease in the metal binding affinity, as measured by isothermal titration calorimetry, and a large reduction in enzyme catalytic efficiencies. This study revealed the vital role of the ligand E349 in enzyme function. Substitution of this residue by alanine resulted in loss of activity. The E349G variant retained 5% activity for the coupled reaction, suggesting that coordinating water may be able to support activation of the *trans* bound dioxygen upon substrate binding. The reaction catalyzed by the H183A variant was fully uncoupled. H183A variant catalytic activity resulted in protein cleavage between Ile^{267} Ala^{268} and the production of an N-terminal fragment. The H266A variant was able to produce 4-hydroxyphenylacetate (HPA), demonstrating that decarboxylation had occurred but that there was no subsequent product formation. Structural modeling of the variant enzyme with bound dioxygen revealed the rearrangement of the coordination environment and the dynamic behaviour of bound dioxygen in the H266A and H183A variants, respectively. These models suggest that the residues regulate the geometry of the reactive oxygen intermediate during the oxidation reaction. The mutagenesis and structural simulation studies demonstrate the critical and unique role of each ligand in the function of HPPD, and which correlates with their respective coordination position.

Introduction

4-Hydroxylphenylpyruvate dioxygenase (HPPD, EC 1.13.11.27) is an important enzyme in the tyrosine catabolic pathway, which catalyzes the oxidative conversion of 4-hydroxyphenylpyruvate (HPP) to homogentisate (HG) with concomitant release of CO_2. Mutations in the encoding gene of human HPPD result in metabolic disorders [1-3]. The enzyme is also a molecular target for potent herbicides because in plants the HG product is an essential precursor for the biosynthesis of redox cofactors such as plastoquinones and tocochromanols [4-7].

HPPD is a member of the non-haem Fe(II)/2-oxoacid-dependent oxygenase family. The majority of these enzymes catalyze the oxidative decarboxylation of 2-oxoglutarate (2-OG) to generate a high-energy iron species, which is subsequently used to effect substrate oxidation. In the case of HPPD, the 2-oxoacid is not contained within a cosubstrate but is located within the pyruvate moiety of the HPP substrate molecule. The catalytic mechanism for the enzyme is complicated and not fully understood, but it is proposed to involve oxidative decarboxylation of HPP using dioxygen to yield HPA and a high reactive Fe(IV)-oxo intermediate. The latter mediates hydroxylation of the aromatic ring, which is followed by a 1,2-shift of the acetyl group to form the HG product [8, 9] (Fig. 1A). During this reaction two atoms of oxygen from dioxygen are incorporated into the product, in the aromatic hydroxyl group and the carboxyl group [10].

Mononuclear non-haem iron(II) enzymes catalyze a diverse range of oxidative reactions but share a strictly conserved structural motif, the 2-His-1-carboxylate (Asp/Glu) facial triad, which is used to coordinate the active site metal [11]. Many of these enzymes, including deacetoxycephalosporin C synthase, clavaminic acid synthase, and taurine/2-OG dioxygenase, are folded into the conserved "jellyroll" protein fold [12-14]. Recently, a number of crystal structures revealed flexibility in the metal coordination in other non-haem iron oxygenase belonging to the cupin protein family [15-19]. These enzymes coordinate the metal centre in different ways to the classical 2His-1-carboxylate motif, with changes including the replacement of the coordinated carboxylate by a histidine, coordination of the iron through two, three or four histidine residues, or coordination by three histidines and one glutamate. These types of coordination are found in the protein structures of halogenase, cysteine dioxygenase, carotene oxygenase and quercetin dioxygenase, respectively [20-23]. Changing metal coordination might result in a change in mechanism for these non-haem iron-dependent enzymes.

The critical role of the 2-His-1-carboxylate motif as the Fe^{2+} binding ligands in these enzymes has been confirmed by site-directed mutagenesis, supporting the crystallographic studies [24-27]. Interestingly, the carboxylate variants of the Factor Inhibiting Hypoxia-Inducible Factor (FIH) exhibited turnover of 2-OG, in particular the D201G variant. This variant was able to coupled 2-OG turnover with hydroxylation of the peptide substrate [27]. The crystal structure of the variant FIH in complex with the peptide substrate demonstrated that two His residues alone are sufficient to coordinate the metal within the active site in this enzyme. The binding manner resembles that observed in the reported structure of non-haem iron-dependent halogenase SyrB2, in which the carboxylate ligand is replaced by a halide ion [20]. These studies highlight the potential structural flexibility of the facial triad in metal coordination.

Unlike the jellyroll motif in 2-OG dependent oxygenases, HPPD is topologically similar to the extradiol dioxygenases with two barrel-shaped domains [28, 29]. The active site of HPPD is located in the C-terminal domain, which is buried within the β-barrel structure containing a similar triad motif for metal binding [30-34]. The metal coordination ligands of His183, His266 and Glu349 are strictly conservative across the HPPD homologues, although their overall sequences share less than 30% identity (Fig. 1B). These three ligands were ligated to iron in a five-coordinate, distorted square-pyramidal arrangement or octahedral geometry, as reported in the ternary complex structure of HPPD from *S. avermitilis* and *R. novegicus*, respectively [30, 34]. In these structures, the two oxygen atoms of the inhibitor coordinate to the metal ion *trans* to

the His and Glu ligands, respectively. Similar coordination geometries were observed in the structure of the hydroxymandelate synthase (HMS)-4-hydroxymandelate (HMA) complex, in which a distorted trigonal bipyramidal arrangement is found. HMS is related to HPPD and catalyzes the conversion of the HPP substrate to HMA [35]. The arrangement of ligands and inhibitor/HMA in metal coordination is similar to that of other 2-OG dependent oxygenases and the O_2 is assumed to occupy the sixth binding site of the metal [12, 36, 37]. Although the structure of HPPD in complex with HPP is not available, recent site-directed mutagenesis studies of active site residues and quantum mechanical/molecular mechanical (QM/MM) theoretical calculations have shed light on the binding of HPP in the active site of carrot HPPD [38]. In this model, the HPP is coordinated in a different arrangement in which the oxygen atoms of carboxylate and keto groups of HPP bind *trans* to 2 His ligands, and the dioxygen molecule is assumed to bind opposite to the Glu ligand. Structural, spectroscopic and computational studies have suggested that the binding of substrate activates the metal centre to attack by dioxygen [14, 16, 17, 19, 39]. The donor interaction of the 2-oxoacid with the metal primes the activation of dioxygen by the metal [40]. Although the binding site of dioxygen molecule in the facial triad is flexible as revealed by structural studies, the relationship between the reactivity of the bound dioxygen and the identity of the respective *trans* ligand remains unclear [14, 16, 17, 19].

To better understand the contribution of facial triad to the properties of metal coordination and enzyme function, mutation analysis of human HPPD was carried out. This study revealed that one Glu and one His residue but not two His residues are sufficient for catalytic function. The Glu ligand in the triad plays a critical role in catalytic function and the His ligands regulate the coupling of the reaction and avoid other possible side reactions.

Experimental Procedures

Materials

The QuikChange mutagenesis kit was purchased from Stratagene. Q-Sepharose, SOURCE 15PHE and Sephacryl HR-100 were obtained from GE Healthcare. All other chemicals and buffers were purchased from the Merck, the Sigma-Aldrich Chemical Co. or J. T. Baker and were of the highest purity available. Aqueous solutions were made up in Milli-Q 18.2 MΩ cm^{-1} water and pH adjusted with NaOH or HCl. Solutions and equipment for molecular biology were purchased sterile or sterilized by autoclaving at 121ºC and 15 PSI for 20 minutes or filtration through a 0.22 μ filter.

Site-directed mutagenesis

The variants of H183A, H266A, E349A, E349G, and E349Q were generated by using the QuikChange mutagenesis kit with *Pfu* DNA polymerase and the vector of p*Trc*-HPPD as template [41]. Two complementary primers including the desired mutations were used for PCR (Table S1). The variant-containing vectors were transformed into *E. coli* DH5α competent cells and the presence of the desired mutation was confirmed by DNA sequencing of the coding region.

Protein purification

The overexpression and purification of recombinant wild-type and variant HPPD enzymes were carried out as reported previously [41]. In brief, the supernatant of crude cell extract were loaded onto Q-Sepharose anion exchanger column (26 x 150 mm) equilibrated in 50 mM Tris-HCl buffer, pH 7.5, 1 mM EDTA and 1 mM DTT, and eluted with the same buffer. Ammonium sulfate stock solution was added to pooled fractions to give a final concentration of 1.2 M, and the solution was loaded onto a hydrophobic interaction column (Source™ 15PHE, 16 x 100 mm) pre-equilibrated in buffer containing 10% (v/v) glycerol and 1.2 M ammonium sulfate. Protein was eluted with a 1.2 – 0 M ammonium sulfate gradient. The pooled fractions were loaded onto S-100 Sephacryl column (26 x 900 mm) equilibrated with 50 mM Tris-HCl buffer, pH 7.5. Fractions exhibited the highest purity protein, as determined by 10% SDS-PAGE were pooled and

concentrated. Protein concentrations are determined by the method of Bradford [42]. The mass of the purified proteins were analyzed by Mass Spectrometry to confirm the mutation. The metal contents of the purified proteins were determined using inductively coupled plasma-high resolution mass spectrometry (ICPMS) (Perkin Elmer NexION 300S). The metal contents of buffer were also measured for correction.

Enzyme activity measurements

The activity of HPPD was measured using both the Oxygraph and HPLC assays [41]. The oxygen consumption assay was performed in an Oxygraph apparatus equipped with a Clark-type electrode (Hansatech, U.K.). The reaction mixtures containing 5 μg HPPD, 0.2 mM ascorbate and 0.2 mM $FeSO_4$ in 0.1 M Tris-acetate buffer, pH 6.5, which were incubated for 1 min at 37 ^oC, followed by addition of 1 mM HPP to initiate the measurement. The oxygen consumption rates were corrected for the reaction without enzyme. The kinetic assays were carried out at variable concentrations of HPP (0.01 to 2 mM) or $FeSO_4$ (0.01 to 0.4 mM).

The HPLC assay is used to determine HG product formation. Reaction mixtures containing 5 μg of HPPD, 1 mM ascorbate, 1 mM FeSO4, 1 mM HPP in 0.1 M Tris-acetate, pH 6.5, were incubated for 5 min at 37 ^oC with shaking. Following by filtration using centrifugation at 8000 *g* (Amicon Ultra-0.5, 10 kDa) to remove the protein, the product was analyzed by HPLC on a C18 column (4.6 x 250 mm, 5-μm particle size; ODS HYPERSIL) at a flow rate of 1 mL/min. The solvents used were 0.1% TFA (v/v) for buffer A and 80% acetonitrile (v/v) /0.07% TFA (v/v) for buffer B following the elution conditions reported previously [41]. The elution of product was monitored at 230 nm [29]. The eluted product of HG and HPA were identified using the mass spectrometry (Waters 2695 separation module and Micromass ZQ).

Mass spectrometry measurements

Wild-type, H183A, H266A, or E349Q variant proteins were collected after the reaction containing 1 mM HPP or not, and subjected to electrophoresis on a denaturing polyacrylamide gel and stain using Coomassie Brilliant Blue R-250. The protein bands in the gel were excised and in-gel digestion performed according to the reported protocol [43]. In brief, the gel pieces were washed with aq. ammonium bicarbonate (25 mM) in methanol [40% (v/v)] and acetonitrile [50% (v/v)], reduced with dithiothreitol (10 mM) for 30 min at 56 ^oC and alkylated with iodoacetamide (50 mM) in aq. ammonium bicarbonate (50 mM) for 30 min in the dark. The gel pieces were washed and dried in a SpeedVac, and incubated with 10 μL of trypsin solution (12.5 ng/μL) in aq. ammonium bicarbonate (25 mM) and acetonitrile [10% (v/v)] for 16 hrs at 37 ^oC. The peptides were extracted with formic acid [5% (v/v)] in acetonitrile [50% (v/v)] and dried in a SpeedVac. Peptides were resuspended in acetonitrile [50% (v/v)] supplemented with formic acid [0.1% (v/v)] and mixed (1:1) with the matrix solution (5 mg/mL of 2,5-dihydroxybenzoic acid in the same solution), and then spotted onto a target plate and left to dry. The samples were analyzed using a MALDI TOF/TOF mass spectrometer (Bruker AutoflexIII, Breman, Germany) equipped with a 200 Hz SmartBean Laser in positive ion mode with delayed extraction in the reflector mode. The FlexControl and Flex-Analysis (Bruker Daltonik, version 3.0) were used for data acquisition and processing. Mascot search engine (Matrix Science, UK) combined with peptide mass fingerprinting and MS/MS datasets were performed for protein database searches via Biotools 3.1 (Bruker).

Isothermal titration calorimetry (ITC) measurements

The binding affinity of metal ion with wild-type and variant HPPD were determined using the iTC200 calorimeters (MicroCal, Northampton, MA). Titrations were performed at 298 ^oK by injection of 1-2 μL of $CoCl_2$ into 200 μL of proteins in 50 mM Tris-HCl buffer, pH 7.5. The interval between each injection was 200 s to allow the system to reach equilibrium. The heat of each ligand dilution experiment were measured in separate runs and subtracted from the

experimental heat of protein-$CoCl_2$ titration. Integrated heat from each injection was analyzed using the MicroCal Origin software (version 7.0) by fitting the data to a one-site binding model.

Building of variant models

All simulations were performed using the Discovery Studio 4.5 software (Accelrys Inc.). The modelled structure of human HPPD (PDB code: 3ISQ) [32] in complex with HPP and dioxygen was used as the template to generate the models of variant HPPD using the Built Mutants protocol followed by energy minimization with the algorithm of smart minimization until the gradient tolerance was satisfied (RMS Gradient ~ 0.1 kcal/mol/Å). They were then applied to the QM/MM calculations using the Minimization (QM-MM) protocol. Residues located outside 5 Å distance of 4-HPP were set with atom constraints. The metal ion, HPP, dioxygen and the side-chains of H183, H266, and E349 were defined as the quantum atoms. The electronic spin state in DMol3 was set as "auto". The PBE function and coarse convergence criteria were used in DMol3 settings. All other parameters of the protocol were used with their default settings.

Molecular Dynamics (MD) simulations were run with the standard dynamics cascade protocol in the CHARMm force field. The complexed structures of wild-type and variant HPPD were energy minimized using the QM-MM protocol and solvated in an orthorhombic box with a minimum distance of 7 Å from the boundary using the Explicit Periodic Boundary model. Counter ions (Na^+ and Cl^- ions) were added to neutralize the system. All atoms of the protein complex was set constraint, then the whole system was subjected to energy minimization for 1000 steps by Steepest Descent followed by Adopted Basis NR for 2000 steps. Heating of the system were carried out from 50 to 300 ^oK in 2 ps MD simulations followed by equilibration for 2 ps at 300 ^oK. Simulation in the production phase employed the Berendsen coupling algorithm for 100 ps at NVT without any atom constraints. All bonds involving hydrogens in the simulation were constrained by the Shake algorithm. The resulted trajectories after MD were selected to run energy minimization by QM-MM protocol.

Results

Activity of wild-type and variant enzymes

Purification of recombinant wild-type and variant HPPD yielded a pure protein, as judged by SDS-PAGE. The metal content that measured in the purified proteins was very low ($\leq$ 0.05 atoms/monomer) (Table S2) [44]. Circular dichroism analysis showed no gross changes in the secondary structure of enzymes after mutation of these residues (Fig. S1). Using oxygen consumption as a measure of activity, the specific activity of the H183A and H266A variants were about 5 and 10% of the wild-type enzyme, respectively. No detectable activity was observed for the E349A variant (Table 1). In contrast, the E349G and E349Q variants retained about 5% of the activity of the wild-type enzyme.

The steady-state kinetics of HPPD variants were characterized by the rate of oxygen consumption at various concentrations of HPP or metal (Table 2 and Fig. S2). As compared to wild-type enzyme, the K_M values of HPP for H183A and E349G variants are decreased by *ca.* 2-fold, and with a 2-fold increase for the E349Q variant. However, k_{cat} values were reduced by >90% for all variants (Table 2). The k_{cat}/K_M values were decreased by about 9-, 23-, 27- and 32-fold for H183A, H266A, E349G and E349Q variants, respectively, compared to the wild-type enzyme. It seems that a large reduction in the catalytic efficiency has occurred as a result of these mutations.

The activity of wild-type and variant HPPD at variable concentration of Fe^{2+} or Co^{2+} performed a saturation curve (Fig. S2). As compared with wild-type enzyme, no significant changes in the K_d^{Fe} values for the ferrous ion were observed for the H183A and H266A variants, whilst it was increased approximately 7- and 3-fold for the E349G and E349Q variants, respectively (Table 2). When replacing of Fe^{2+} with Co^{2+}, the K_d^{Co} value was decreased by about 30-fold. It seems that the enzyme has a higher binding affinity for Co^{2+} than Fe^{2+} but a lower

activity when using this metal as cofactor. The activity performed in Co^{2+} substituted HPPD was consistent with the extradiol-cleaving catechol dioxygenase [45].

Product analysis of wild-type and variant enzymes

The HG product formation was analyzed using the HPLC assay. The specific activities of the H183A, E349G and E349Q variants were about 1, 5 and 1% of the wild-type enzyme, respectively, whilst no detectable activity was observed for the H266A and E349A variants (Table 1). It is noted that the specific activity for the H183A and E349Q variants as measured by oxygen consumption is 5-fold higher than that measured by HPLC assay, implying only 20% of catalytic cycles are coupled in these variants. No product formation was observed for the H266A variant. This is due to the formation of a stable HPA intermediate rather than the expected HG product. HPLC analysis of the reaction products for the H266A variant confirmed the presence of the HPA intermediate at a retention time of 12.4 minutes (Fig. 2). The amount of the HPA product increased with increasing reaction time and enzyme concentration (Fig. S3). The specific activity for this reaction was calculated from the integrated area of HPA to be *ca.* 0.01 ± 0.004 μmol/min/mg. It is noted that HPA was not produced from the H183A or E349Q variant enzymes, even at greatly extended reaction times or greatly increased enzyme concentrations.

Protein fragmentation after oxidative reaction of variant enzyme

To investigate the possible oxidative modification of the variant enzymes, protein samples from the assay were analyzed by SDS electrophoresis. In the H183A variant an additional band at *ca.* 30 KDa. was observed following incubation with HPP substrate. This fragment was not observed when HPP was omitted from the assay (Fig. 3). This new band accounts for about 10% of the total protein, as judged from the intensity of the band observed by SDS-PAGE analysis. The N-terminal sequence of this new band was determined to be the same as that of intact H183A variant protein, implying it is an N-terminal fragment. The new band was isolated from the gel and subjected to trypsin hydrolysis and MS/MS analysis (Fig. 4). When compared to the peptide mass fingerprint of the wild-type enzyme, an extra peak at m/z of 1977.97 was observed, which corresponds to the peptide sequence ^{250}SQIQEYVDYNGGAGVQHI^{267}. This suggests the Ile267 is at the carboxyl end of the fragment which is cleaved from the variant protein during the catalytic reaction.

Isothermal titration calorimetry analysis

ITC was employed to analysis the metal binding properties of wild-type and variant HPPD. All measurements were carried out by titration of Co^{2+} into the protein to avoid the problem caused by the oxidation of Fe^{2+} in buffer. This ion is also the coordinating metal in the reported X-ray crystal structure of human HPPD [32] and allows some catalytic activity (Table 3). The titration experiment resulted in an exothermic reaction and the integrated heat data of wild-type and variant enzymes were fitted into a one-site binding model (Fig. 5). Based on at least three separate experiments, the averaged dissociation constants for wild-type, H266A, E349A, E349G and E349Q variants were 0.023 ± 0.004, 0.15 ± 0.02, 0.22 ± 0.03, 0.54 ± 0.05 and 0.37 ± 0.11 mM, respectively (Table 3). Dissociation constant could not be measured for the H183A variant because of the low levels of expression of this variant. ITC analysis showed that the binding affinities of H266A, E349A, E349G and E349Q variants with the Co^{2+} were weaker by about 7-, 10, 23- and 16-fold, respectively, than that determined for wild-type enzyme. The binding of these enzymes with the metal is primarily enthalpy-driven (ΔH^o) (data not shown). The standard free energy differences ($\Delta\Delta G^o$) were calculated to be about 1.1, 1.3, 1.8 and 1.6 kcal/mol for the H266A, E349A, E349G and E349Q variants, respectively, by subtraction of the value derived for the wild-type enzyme.

Modeling of wild-type and variant HPPD

Wild-type, H183A, H266A, E349Q and E349G variant HPPD in complex with HPP and O_2 were modeled and geometrically minimized by QM-MM calculation. However, energy minimization by QM-MM protocol was not successful for the model of the E349A variant. In the simulated model of wild-type enzyme, E349, H266 and H183 coordinate in *trans* to O_2, and the oxygen atoms of carboxylate and keto group of HPP, respectively (Fig. 6). The distance measured from the NE2 of H183, NE2 of H266, OE1 of E349, O1 of O_2, and the oxygen atoms of the carboxylate and oxo groups of HPP to the metal were about 2.0, 2.05, 1.95, 1.90, 1.91 and 1.98 Å, respectively. The bond length between two oxygen atoms of O_2 was lengthened from 0.89 to 1.4 Å. Both atoms carry a partial negative charge with the distal oxygen located near the carbon atom of the keto group of HPP at a distance about 2.43 Å. The OE1 of the carboxyl group and 4-hydroxyl group of HPP form hydrogen bonds with the NE2 of Q334 and OE1 of Q251, respectively.

No major changes in the positions of the Cα atoms of the H183A, H266A, E349Q and E349G variants was observed compared to wild-type enzyme. However, movements in the side-chains of H183, H266, E349, Q334, F359 and F364 in the active site were observed (Fig. 6). The positions of the metal ion, dioxygen and HPP were also shifted in these variant HPPD enzymes. The distance between two oxygen atoms of O_2 in these variant enzymes was lengthened as wild-type. The proximal oxygen of O_2 comes close to the metal with the distance about 1.84, 1.83 1.89 and 1.82 Å, and about 2.56, 2.34 2.66 and 2.18 Å between the distal oxygen and the carbon atom of the oxo group of HPP in the H183A, H266A E349Q and E349G variants, respectively. It is noted that the shift of E349 in H266A variant leads to both oxygen atoms of the carboxylate group to coordinate to the metal. This movement also causes the NE2 of Q334 to form hydrogen bond with the OE2 of the carboxyl group of HPP. For the E349Q variant, the amide group of Q349 was rotated about 90 degrees and shifts about 0.78 Å to form hydrogen bonding with the oxo group of HPP. Notably, the empty site in E349G variant was occupied by a water molecule, which coordinates with the metal at a distance of about 2.06 Å.

From the Molecular Dynamics (MD) simulation, conformations of H183A variant were selected for geometrically minimization through QM-MM calculation. One conformation with successful energy minimization showed a different coordination manner between the dioxygen and metal as compared to the model before MD simulation (Fig.6B and C). It is noted that the shift of E349 leads to both oxygen atoms in the carboxylate group to coordinate with the metal. The proximal oxygen of O_2 comes close to the metal at a distance of about 1.83 Å but the distal oxygen placed in a direction away from HPP (Fig. 6C). The distance of the distal oxygen with the carbonyl carbon of I267, the HD2 of H266 and the HB2 of A268 were about 5.07, 3.3 and 2.55 Å, respectively.

Discussion

The strictly conservative structure of human HPPD contains a 2-His-1-Glu facial triad to anchor the Fe^{2+} into the active site for catalysis [32]. The present study demonstrates that mutating the side-chains of the three selected residues resulted in a considerable reduction in enzyme activity. The E349A mutation, in particular, diminished the activity as measured by both oxygen consumption and HG production. The results highlight the vital role of E349 in enzyme function. It is noted that in the absence of HPP, the metal is still bound in the E349A variant protein suggesting that two His residues are sufficient for iron binding consistent with the report for the analogous D201A variant in FIH [27]. However, in HPPD catalytic activity is lost (Table 1). Hence, the carboxylate group of the ligand in the coordination is suggested to be essential for Fe^{2+} binding and subsequently activation of the dioxygen upon substrate binding, the initial step for oxygenase activity of HPPD [19, 39, 40].

It is interesting that the E349G variant possesses residual activity although glycine contains no side-chain to bind with Fe^{2+}. The space left in this site is assumed to enable a water molecule to coordinate with the iron as observed in the crystal structure of the FIH D201G variant complex

[27]. The hydroxylation activity performed on the variant FIH suggests that a bound water molecule is able to fulfill this function. Although the E349G variant HPPD exhibited weak binding affinity with metal, the coordinated water molecule which located in *trans* to the dioxygen molecule, as shown in the simulated model (Fig. 6A), seems to be able to support the activation of dioxygen when substrate is bound and couples decarboxylation and HG product formation.

Substitution of the metal binding ligand might impact on the interaction of the reactive oxygen intermediate in the catalytic reaction. It is noted that although the variants of H183A, H266A and E349Q exhibited residue activity (~5-10% of wild-type enzyme), their activities measured by oxygen consumption and HG product were not equivalent suggesting a significant amount of uncoupled reaction (Table 1). The uncoupled reaction catalyzed by H266A variant produces the HPA intermediate in place of HG product (Fig. 2). In the modeled structure, the H266A variant showed a different coordination environment around the metal, in particular the additional coordination from E349 and the interaction of the side-chain of Q334 with HPP (Fig. 6A). These changes might reduce efficient activation of dioxygen by Fe^{2+} for the initial nucleophilic reaction with the 2-oxo group of HPP. The change in coordination appears to impact on the correct orientation of the Fe(IV)-oxo intermediate for hydroxylation in the aromatic side-chain of HPA. Hence, H266 is assumed to play the role in regulating the geometry of reactive oxygen intermediate for coupling the decarboxylation and hydroxylation reactions.

The mechanism in the uncoupled reaction catalyzed by H183A and E349Q variants seems to be different because no HPA or other product derived from HPP was measured in the reaction solution. Self-hydroxylation is catalyzed by several 2-OG dependent Fe(II) oxygenase, which results in modification of Phe, Tyr or Trp residues located near the active site in the presence of 2-OG but not the primary substrate [46-49]. Isotope labeling experiments suggests the involvement of an Fe(VI)-oxo intermediate in the process and assumes that this reaction is a strategy to protect the enzyme from severe peptide cleavage [46]. However, no hydroxylated residues in the H266A or E349Q variant active sites were observed by MS/MS analysis following reaction in the presence of HPP substrate, suggesting that this uncoupled reaction is unlikely to be a self-inactivation process.

Protein fragmentation was observed following the oxidative reaction catalyzed by H183A variant. This suggests an alternative reactivity of the reactive oxygen intermediate in protein molecule (Fig. 3) [40]. In this reaction the peptide bond between Ile^{267} and Ala^{268} in HPPD was cleaved, which is at a site close to H266. Interestingly, the site for the modified tryptophan residue that generated by self-hydroxylation of 2,4-dichlorophenoxyacetate/2-OG dioxygenase (TfdA) in the presence of cofactor but not substrate is also located adjacent to His113, the equivalent metal-binding ligand [46]. These results reveal the potential sites for side reaction through metal-mediated oxidation. Oxidative fragmentation was also reported for 1-aminocyclopropane-1-carboxylate (ACC) oxidase, which utilizes ascorbate but not a 2-oxoacid as a cosubstrate in the enzyme catalyzed reaction [50]. Fragmentation in ACC oxidase increased following modification of the metal-binding ligands [50].

Modeling studies on the dioxygen bound HPPD H183A complex suggests that two different dioxygen binding modes are possible. In these two modes, the distal oxygen atom is located either facing towards or away from the HPP (Fig. 6B and C, respectively). Thus, substitution at H183 seems to increase the flexibility in the coordination centre leading to the dynamic behaviour of the reactive oxygen intermediate in the reaction [18]. The exact mechanism for the protein fragmentation by the reactive oxygen intermediate remains unclear. However, the irreversible destruction in the H183A variant protein after the oxidative reaction process suggests that this ligand plays an important role in metal ion coordination and hence determines the appropriate orientation of the reactive oxygen intermediate in the oxidative reaction. This appears to be critical for protection of the protein from damage by alternative oxidative reactions.

In the modeled structures, the oxygen atoms in the carboxyl group of E349 take over the

coordination when either H266 or H183 are substituted. This explains the residual activities performed by both variant enzymes and also demonstrated that one Glu and one His are sufficient for HPPD activity. These results contrast with the mutagenesis study on FIH, which suggests that two His residues is required for iron function [27]. This highlights the different roles of each metal binding ligand that acts in the catalysis reaction of HPPD and 2-oxoglutarate-dependent oxygenases. This difference might due to the inclusion of an oxoacid moiety within the HPP substrate. In the FIH structure, the position for 2-OG co-substrate to bidentate coordinated in other dioxygenase is located perpendicular to the Glu and one His ligand, respectively, and the dioxygen is presumed to occupy the sixth binding site *trans* to a His ligand [14, 37, 51]. However, rearrangement of the Fe(VI)-oxo intermediate is required for correct orientation towards the prime substrate that is bound in the vicinity of the metal binding sphere [37, 52]. For HPPD, the coordination site of the dioxygen and the oxo-group of the intermediate seem to stay at the same place, perpendicular to the Glu ligand [38]. This result suggests some flexibility in the metal centered coordination for various chemical transformations. For HPPD, a single 2-oxoacid substrate which coordinates to the metal centre seems to be sufficient for completion of a complicated catalytic reaction.

Substitution in the facial triad of HPPD resulted in about 10-fold reduction in the affinity with metal as measured by ITC (Table 3). From the K_d values for Fe^{2+} in the activity assay, it was noted that only the reaction catalyzed by E349G and E349Q variants were significantly increased (Table 2). However, the K_M values for HPP in the catalytic reaction of these variants is similar to the wild-type enzyme whilst the catalytic efficiencies were substantially reduced (Table 2). The results highlight the critical role of ligand coordination in stabilization of the metal for the catalytic reaction. The different nature of mutation led to the loss of activity for E349A, and the E349G and E349Q mutants that retain residual activity but different kinetic parameter highlight the critical role of the carboxylate group of E349 in metal coordination. Substitution might impact the charge transfer ability from metal to the *trans* bound dioxygen when substrate is bound, which influences the reaction efficiency (Fig. 6) [38]. The reduction in the activity for H183A and H266A mutants were unlikely due to the water molecule which fills the empty space in the A183 or A266 mutation sites. It implies that the metal coordination by only the E349 and H183 or E349 and H266 is sufficient to retain the catalytic function of the enzyme; however, regulation of the reaction in coupled seems to impact. In this structural model, H266 is coordinated in *cis* position to HPP. The mutation appears to alter the efficient interaction of the oxygen intermediate with the phenyl moiety of HPA. However, H183 which is coordinated opposite to the oxo group of HPP seems to play a key role in controlling the oxidative intermediate to prevent self-damage. Therefore, this study reveals the distinct role of each metal binding ligand in the function of HPPD. The functions include controlling the initiation of the oxidative reaction, regulation of the oxygen intermediate during the coupled reaction and prevention of severe side reaction by E349, H266 and H183, respectively. These roles are correlated with their respective coordination positions with respect to bound dioxygen or HPP.

.

Acknowledgements

We thank Miss Hsi-lin Chen for assistance in Mass spectrometry measurements at Institute of Molecular Biology, Academia Sinica, Taiwan and Professor Hao-Ai Shui (the Graduate Institute of Medical Sciences, National Defense Medical Center) for discussion of the MS data.

Funding

This study was supported financially by the National Science Council (NSC 99-2311-B-016-001-MY3), National Defense Medical Bureau (MAB103-M020 and MAB104-031) and Tri-Service General Hospital (TSGH-C103-147 and TSGH-C104-136).

Author contributions

Hwei-Jen Lee and Chih-Wei Huang designed the experiments. Chih-Wei Huang, Hsiu-Chen Liu, Chia-Pei Shen, Yi-Tong Chen and Sung-Jai Lee performed the experiments. Chih-Wei Huang, Matthew D. Lloyd and Hwei-Jen Lee analysed the data. Chih-Wei Huang and Hwei-Jen Lee wrote the manuscript

Reference:

1. Tomoeda K., Awata H., Matsuura T., Matsuda I., Ploechl E., Milovac T., Boneh A., Scott C.R., Danks D.M. and Endo F. (2000) Mutations in the 4-hydroxyphenylpyruvic acid dioxygenase gene are responsible for tyrosinemia type III and hawkinsinuria. *Mol. Genet. Metab.* **71**:506-510.
2. Holme E. and Lindstedt S. (1998) Tyrosinaemia type I and NTBC (2-(2-nitro-4-trifluoromethylbenzoyl)-1,3-cyclohexanedione). *J. Inherit. Metab. Dis.* **21**:507-517.
3. Lindstedt S., Holme E., Lock E.A., Hjalmarson O. and Strandvik B. (1992) Treatment of hereditary tyrosinaemia type I by inhibition of 4-hydroxyphenylpyruvate dioxygenase. *Lancet.* **340**, 813-817.
4. Goodwin T.W. and Mercer E.I. (1983) *Introduction to Plant Biochemistry*. Pergamon Press, Sydney.
5. Garcia I., Job D. and Matringe M. (2000) Inhibition of p-hydroxyphenylpyruvate dioxygenase by the diketonitrile of isoxaflutole: a case of half-site reactivity. *Biochemistry.* **39**, 7501-7507.
6. Mitchell G., Bartlett D.W., Fraser T.E., Hawkes T.R., Holt D.C., Townson J.K. and Wichert, R.A. (1999) Mesotrione: a new selective herbicide for use in maize. *Pest Manage Sci.* **57**:120-128.
7. Schulz A., Ort O., Beyer P. and Kleinig H. (1993) SC-0051, a 2-benzoyl-cyclohexane-1,3-dione bleaching herbicide, is a potent inhibitor of the enzyme p-hydroxyphenylpyruvate dioxygenase. *FEBS Lett.* **318**:162-166.
8. Crouch N.P., Adlington R.M., Baldwin J.E., Lee M.H. and MacKinnon C.H. (1997) A mechanistic rationalisation for the substrate specificity of recombinant mammalian 4-hydroxyphenylpyruvate dioxygenase. *Tetrahedron.* **53**:6993-7010.
9. Moran G.R. (2005) 4-Hydroxyphenylpyruvate dioxygenase. *Arch. Biochem. Biophys.* **433**:117-128.
10. Lindblad B., Lindstedt G. and Lindstedt S. (1970) The mechanism of enzymatic formation of homogentisate from p-hydroxyphenylpyruvate. *J. Am. Chem. Soc.* **92**:7446-7449.
11. Hegg E.L. and Que L.J. (1997) The 2-His-1-carboxylate facial triad: a emerging structural motif in mononuclear non-heme iron(II) enzymes. *Eur. J. Biochem.* **250**:625-629.
12. Elkins J.M., Ryle M.J., Clifton I.J., Dunning Hotopp J.C., Lloyd J.S., Burzlaff N.I., Baldwin J.E., Hausinger R.P. and Roach P.L. (2002) X-ray crystal structure of *Escherichia coli* taurine/alpha-ketoglutarate dioxygenase complexed to ferrous iron and substrates. *Biochemistry.* **41**:5185-5192.
13. Valegard K., van Scheltinga A.C., Lloyd M.D., Hara T., Ramaswamy S., Perrakis A., Thompson A., Lee H.J., Baldwin J.E., Schofield C.J. and Hajdu J., Andersson I. (1998) Structure of a cephalosporin synthase. *Nature.* **394**:805-809.
14. Zhang Z., Ren J., Stammers D.K., Baldwin J.E., Harlos K. and Schofield C.J. (2000) Structural origins of the selectivity of the trifunctional oxygenase clavaminic acid synthase. *Nature Struct. Biol.* **7**:127-133.
15. Karlsson A., Parales J.V., Parales R.E., Gibson D.T., Eklund H. and Ramaswamy S. (2003) Crystal structure of naphthalene dioxygenase: side-on binding of dioxygen to iron. *Science.* **299**:1039-1042.
16. Roach P.L., Clifton I.J., Hensgens C.M., Shibata N., Schofield C.J., Hajdu J. and Baldwin J.E. (1997) Structure of isopenicillin N synthase complexed with substrate and the mechanism of penicillin formation. *Nature.* **387**:827-830.
17. Sato N., Uragami Y., Nishizaki T., Takahashi Y., Sazaki G., Sugimoto K., Nonaka T., Masai E., Fukuda M. and Senda T. (2002) Crystal structures of the reaction intermediate and its homologue of an extradiol-cleaving catecholic dioxygenase. *J. Mol. Biol.* **321**:621-636.
18. Zhang Z., Ren J., Harlos K., McKinnon C.H., Clifton I.J. and Schofield C.J. (2002) Crystal structure of a clavaminate synthase-Fe(II)-2-oxoglutarate-substrate-NO complex: evidence for metal centered rearrangements. *FEBS Lett.* **517**:7-12.
19. Koehntop K.D., Emerson J.P. and Que L., Jr. (2005) The 2-His-1-carboxylate facial triad: a versatile platform for dioxygen activation by mononuclear non-heme iron(II) enzymes. *J. Biol.*

Inorg. Chem. **10**:87-93.
20. Blasiak L.C., Vaillancourt F.H., Walsh C.T. and Drennan C.L. (2006) Crystal structure of the non-haem iron halogenase SyrB2 in syringomycin biosynthesis. *Nature.* **440**:368-371.
21. McCoy J.G., Bailey L.J., Bitto E., Bingman C.A., Aceti D.J., Fox B.G. and Phillips G.N., Jr. (2006) Structure and mechanism of mouse cysteine dioxygenase. *Proc. Natl. Acad. Sci. U. S. A.* **103**:3084-3089.
22. Kloer D.P., Ruch S., Al-Babili S., Beyer P. and Schulz G.E. (2005) The structure of a retinal-forming carotenoid oxygenase. *Science.* **308**:267-269.
23. Gopal B., Madan L.L., Betz S.F. and Kossiakoff A.A. (2005) The crystal structure of a quercetin 2,3-dioxygenase from *Bacillus subtilis* suggests modulation of enzyme activity by a change in the metal ion at the active site(s). *Biochemistry.* **44**:193-201.
24. Doan L.X., Hassan A., Lipscomb S.J., Dhanda A., Zhang Z. and Schofield C.J. (2000) Mutagenesis studies on the iron binding ligands of clavaminic acid synthase. *Biochem. Biophys. Res. Commun.* **279**:240-244.
25. Grzyska P.K., Muller T.A., Campbell M.G. and Hausinger R.P. (2007) Metal ligand substitution and evidence for quinone formation in taurine/alpha-ketoglutarate dioxygenase. *J. Inorg. Biochem.* **101**:797-808.
26. Sim J. and Sim T. S. (2000) Mutational evidence supporting the involvement of tripartite residues His183, Asp185, and His243 in *Streptomyces clavuligerus* deacetoxycephalosporin C synthase for catalysis. *Biosci. Biotech. Biochem.* **64**:828-832.
27. Hewitson K.S., Holmes S.L., Ehrismann D., Hardy A.P., Chowdhury R., Schofield C.J. and McDonough M.A. (2008) Evidence that two enzyme-derived histidine ligands are sufficient for iron binding and catalysis by factor inhibiting HIF (FIH). *J. Biol. Chem.* **283**:25971-25978.
28. Han S., Eltis L.D., Timmis K. N., Muchmore S.W. and Bolin J.T. (1995) Crystal structure of the biphenyl-cleaving extradiol dioxygenase from a PCB-degrading pseudomonad. *Science.* **270**:976-980.
29. Kita A., Kita S., Fujisawa I., Inaka K., Ishida T., Horiike K., Nozaki M. and Miki, K. (1999) An archetypical extradiol-cleaving catecholic dioxygenase: the crystal structure of catechol 2,3-dioxygenase (metapyrocatechase) from *Pseudomonas putida* mt-2. *Structure.* **7**:25-34.
30. Brownlee J.M., Johnson-Winters K., Harrison D.H. and Moran G.R. (2004) Structure of the ferrous form of (4-hydroxyphenyl)pyruvate dioxygenase from *Streptomyces avermitilis* in complex with the therapeutic herbicide, NTBC. *Biochemistry.* **43**:6370-6377.
31. Fritze I.M., Linden L., Freigang J., Auerbach G., Huber, R. and Steinbacher, S. (2004) The crystal structures of Zea mays and Arabidopsis 4-hydroxyphenylpyruvate dioxygenase. *Plant Physiol.* **134**:1388-1400.
32. Pilka E.S., Shafqat N., Cocking R., Bray J.E., Krojer T., Pike A.C.W., von Delft F., Yue W.W., Arrowsmith C.H., Weigelt J., Edwards A., Bountra C., Oppermann U. and Kavanagh K.L. Crystal structure of human 4-Hydroxyphenylpyruvate dioxygenase, *Submitted (SEP-2009) to the PDB data bank*. (PDB ID: 3ISQ)
33. Serre L., Sailland A., Sy D., Boudec P., Rolland A., Pebay-Peyroula E. and Cohen-Addad C. (1999) Crystal structure of *Pseudomonas fluorescens* 4-hydroxyphenylpyruvate dioxygenase: an enzyme involved in the tyrosine degradation pathway. *Structure.* **7**:977-988.
34. Yang C., Pflugrath J.W., Camper D.L., Foster M.L., Pernich D.J. and Walsh T.A. (2004) Structural basis for herbicidal inhibitor selectivity revealed by comparison of crystal structures of plant and mammalian 4-hydroxyphenylpyruvate dioxygenases. *Biochemistry.* **43**:10414-10423.
35. Brownlee J., He P., Moran G.R. and Harrison D.H. (2008) Two roads diverged: the structure of hydroxymandelate synthase from *Amycolatopsis orientalis* in complex with 4-hydroxymandelate. *Biochemistry.* **47**:2002-2013.
36. Elkins J.M., Hewitson K.S., McNeill L.A., Seibel J.F., Schlemminger I., Pugh C.W., Ratcliffe P.J. and Schofield C.J. (2003) Structure of factor-inhibiting hypoxia-inducible factor (HIF) reveals mechanism of oxidative modification of HIF-1 alpha. *J. Biol. Chem.* **278**:1802-1806.

37. Yu B., Edstrom W.C., Benach J., Hamuro Y., Weber P.C., Gibney B.R. and Hunt J.F. (2006) Crystal structures of catalytic complexes of the oxidative DNA/RNA repair enzyme AlkB. *Nature.* **439**:879-884.
38. Raspail C., Graindorge M., Moreau Y., Crouzy S., Lefebvre B., Robin A.Y., Dumas R. and Matringe M. (2011) 4-Hydroxyphenylpyruvate dioxygenase catalysis: identification of catalytic residues and production of a hydroxylated intermediate shared with a structurally unrelated enzyme. *J. Biol. Chem.* **286**:26061-26070.
39. Solomon E.I., Decker A. and Lehnert N. (2003) Non-heme iron enzymes: contrasts to heme catalysis. *Proc. Natl. Acad. Sci. U. S. A.* **100**:3589-3594.
40. Diebold A.R., Brown-Marshall C.D., Neidig M.L., Brownlee J.M., Moran G.R. and Solomon E.I. (2011) Activation of alpha-keto acid-dependent dioxygenases: application of an {FeNO}7/{FeO2}8 methodology for characterizing the initial steps of O_2 activation. *J. Am. Chem. Soc.* **133:**18148-18160.
41. Lin J.F., Sheih Y.L., Chang T.C., Chang N.Y., Chang C.W., Shen C.P. and Lee H.J. (2013) The interactions in the carboxyl terminus of human 4-hydroxyphenylpyruvate dioxygenase are critical to mediate the conformation of the final helix and the tail to shield the active site for catalysis, *PloS One.* **8:**e69733.
42. Fielding A.J., Lipscomb J.D. and Que L., Jr. (2012) Characterization of an O_2 adduct of an active cobalt-substituted extradiol-cleaving catechol dioxygenase. *J. Am. Chem. Soc.* **134:**796-799.
43. Shevchenko A., Tomas H., Havlis J., Olsen J. V. and Mann M. (2006) In-gel digestion for mass spectrometric characterization of proteins and proteomes. *Nature protocols.* **1:**2856-2860.
44. Johnson-Winters K., Purpero V.M., Kavana M., Nelson T. and Moran G.R. (2003) (4-Hydroxyphenyl)pyruvate dioxygenase from *Streptomyces avermitilis*: the basis for ordered substrate addition. *Biochemistry.* **42**:2072-2080.
45. Fielding A.J., Kovaleva E.G., Farquhar E.R., Lipscomb J.D. and Que L., Jr. (2011) A hyperactive cobalt-substituted extradiol-cleaving catechol dioxygenase. *J. Biol. Inorg. Chem.* **16**:341-355.
46. Liu A., Ho R. Y., Que L., Jr., Ryle M.J., Phinney B.S. and Hausinger R.P. (2001) Alternative reactivity of an alpha-ketoglutarate-dependent iron(II) oxygenase: enzyme self-hydroxylation. *J. Am. Chem. Soc.* **123**:5126-5127.
47. Ryle M.J., Liu A., Muthukumaran R.B., Ho R.Y., Koehntop K.D., McCracken J., Que L., Jr. and Hausinger R.P. (2003) O_2- and alpha-ketoglutarate-dependent tyrosyl radical formation in TauD, an alpha-keto acid-dependent non-heme iron dioxygenase. *Biochemistry.* **42**:1854-1862.
48. Bradley F.C., Lindstedt S., Lipscomb J.D., Que L., Jr., Roe A.L. and Rundgren M. (1986) 4-Hydroxyphenylpyruvate dioxygenase is an iron-tyrosinate protein. *J. Biol. Chem.* **261**:11693-11696.
49. Chen Y.H., Comeaux L.M., Eyles S.J. and Knapp M.J. (2008) Auto-hydroxylation of FIH-1: an Fe(II), alpha-ketoglutarate-dependent human hypoxia sensor. *Chem Commun (Camb).* 4768-4770.
50. Zhang Z., Liu H. and Deng J. (1996) A Glucose Biosensor Based on Immobilization of Glucose Oxidase in Electropolymerized o-Aminophenol Film on Platinized Glassy Carbon Electrode. *Anal. Chem.* **68**:1632-1638.
51. Lloyd M.D., Lee H.J., Harlos K., Zhang Z.H., Baldwin J.E., Schofield C.J., Charnock J.M., Garner C.D., Hara T., Terwisscha van Scheltinga A. C., Valegard K., Viklund J. A., Hajdu J., Andersson I., Danielsson A. and Bhikhabhai R. (1999) Studies on the active site of deacetoxycephalosporin C synthase. *J. Mol. Biol.* **287**:943-960.
52. Quesne M. G., Latifi R., Gonzalez-Ovalle L. E., Kumar D. and de Visser S. P. (2014) Quantum mechanics/molecular mechanics study on the oxygen binding and substrate hydroxylation step in AlkB repair enzymes *Chemistry.* **20**:435-446.

Table 1. Specific activities for wild-type and variant HPPD

	Oxygen consumption (μmol/min/mg)	HG production (μmol/min/ mg)
WT	2.1 ± 0.09	1.7 ± 0.08
H183A	0.1 ± 0.02	0.02 ± 0.004
H266A	0.2 ± 0.07	ND
E349A	ND	ND
E349G	0.09 ± 0.005	0.08 ± 0.01
E349Q	0.1 ± 0.01	0.02 ± 0.002

*The Oxygraph and HPLC were used to assay activity by measuring oxygen consumption and HG production, respectively. The reported values are means ± S.D. for three independent experiments. ND, no detectable activity.

Table 2. Apparent kinetic parameters

	HPP			metal	
	k_{cat} (s^{-1})	K_M (mM)	k_{cat}/K_M	K_d^{Fe} (mM)	K_d^{Co}(mM)
WT	3.3 ± 0.4	0.2 ± 0.05	16 ± 3	0.03 ± 0.003	0.001 ± 0.0003
H183A	0.16 ± 0.004	0.09 ± 0.004	1.8 ± 0.03	0.04 ± 0.006	-
H266A	0.13 ± 0.01	0.18 ± 0.02	0.7 ± 0.04	0.04 ± 0.01	-
E349G	0.05 ± 0.002	0.1 ± 0.01	0.6 ± 0.03	0.2 ± 0.03	-
E349Q	0.2 ± 0.01	0.4 ± 0.1	0.5 ± 0.1	0.09 ± 0.02	-

*The oxygen consumption was used to assay activity. The parameters for HPP and metal were obtained by the fitting the kinetic data to the Michaelis-Menten and saturation curve equation, respectively. The K_d is the binding constant that represents the metal concentration needed to achieve half value of the maxima velocity. The reported values are means ± S.D. for three independent experiments.

Table 3. Binding constants of cobalt ion with wild-type and variant HPPD.

	K_d (mM)	ΔG (kcal/mol)
WT	0.023 ± 0.004	-6.3 ± 0.1
H266A	0.15 ± 0.02	-5.2 ± 0.1
E349A	0.22 ± 0.03	-5.0 ± 0.1
E349G	0.54 ± 0.05	-4.5 ± 0.1
E349Q	0.37 ± 0.11	-4.7 ± 0.5

The reported values are means ± S.D. for three independent experiments.

Figure legends

Figure 1: (A) The proposed reaction mechanism catalyzed by human HPPD (*h*HPPD) [9]. (B) Sequence alignment of HPPD and homologous enzymes from different species. Fully conservative residues are highlighted and the facial triad is colored as dark grey. Location of these residues in the β-strands, defined based on the topology of human HPPD structure (PDB code: 3ISQ), are rendered as arrows [32]. Abbreviations used: *h*HPPD, *Homo sapiens* (human) HPPD; *r*HPPD, *Rattus norvegicus* (rat) HPPD; *sa*HPPD, *Streptomyces avermitilis* HPPD; *at*HPPD, *Arabidopsis thaliana* HPPD; *ao*HMS, *Amycolatopsis orientalis* HMS; *zm*HPPD, *Zea mays* HPPD; *Pf*HPPD, *Pseudomonas fluorescens* 4-HPPD.

Figure 2. HPLC analysis of the product formed by WT and variant HPPD. These assays are incubated at 30 ^{o}C for 5 min containing 30 μg proteins. Control assay includes all reaction mixture except enzyme. The elution profile for standard HG and HPA were shown as dark and gray lines, respectively.

Figure 3. SDS-PAGE analysis of HPPD variants after oxidative reaction. The solution for control (C) and reaction (R) experiments include 1 mM $FeSO_4$, 1 mM ascorbate and 18 μg protein in 0.1 M Tris-acetate buffer, pH 6.5, in the absence and presence of 1 mM HPP, respectively. Reactions were carried out for 5 min at 30 ^{o}C. The additional band was highlighted as black rectangular line.

Figure 4. MS/MS analysis of the tryptic peptide (Ser250-Ile267) obtained from H183A variant HPPD. The sample corresponding to the additional band as shown in Fig 3 was excised from the gel, digested with trypsin and submitted for MS/MS analysis. (A) The peptide mass fingerprint of the wild-type and the fragment from H183A variant. The additional peptide fragment is highlighted as arrow. (B) The spectrum shows the MS/MS sequencing at m/z of 1977.97 with singly charged y and b fragment ions.

Figure 5. ITC analysis the binding of Co^{2+} to wild-type and variant HPPD. The upper panels show the calorimetric titration of 60, 83, 63 and 157 μM of wild-type (A), H266A (B) and E349G (C) E349Q (D) variant HPPD with 1, 5, 10 and 20 mM of Co^{2+}, respectively. The lower panels display the integrated heat data as a function of Co^{2+}/protein molar ratio.

Figure 6. The simulated models of wild-type and variant HPPD in complex with HPP and dioxygen. (A) Superimposition of the wild-type and H183A, H266A, E349Q and E349G variants that shown as stick models in green, cyan, yellow, magentas and gray, respectively. The metal, HPP and dioxygen is represented by a sphere and stick model, respectively. Hydrogen bond interactions are shown as dotted green lines. (B) and (C), the H183A variant. The protein is shown as cartoon and colored gray. HPP and dioxygen are shown as stick model and colored yellow and red, respectively. The red circle highlights the different orientation of ligands in the metal binding sphere.

CW Huang et al., Fig. 1

(A)

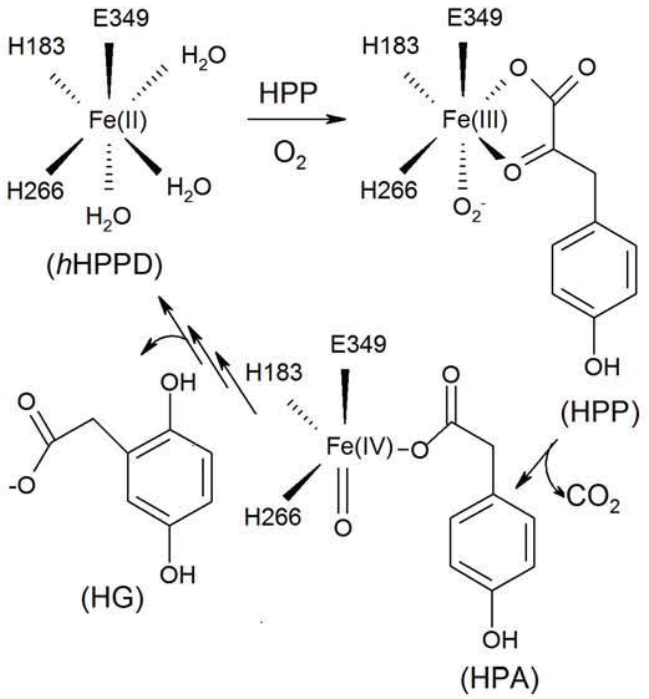

(B)

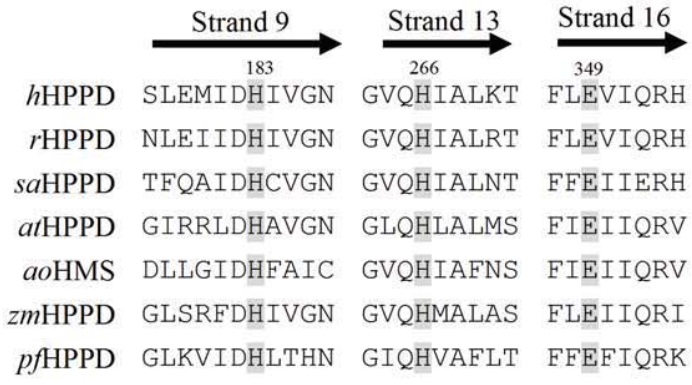

CW Huang et al., Fig. 2

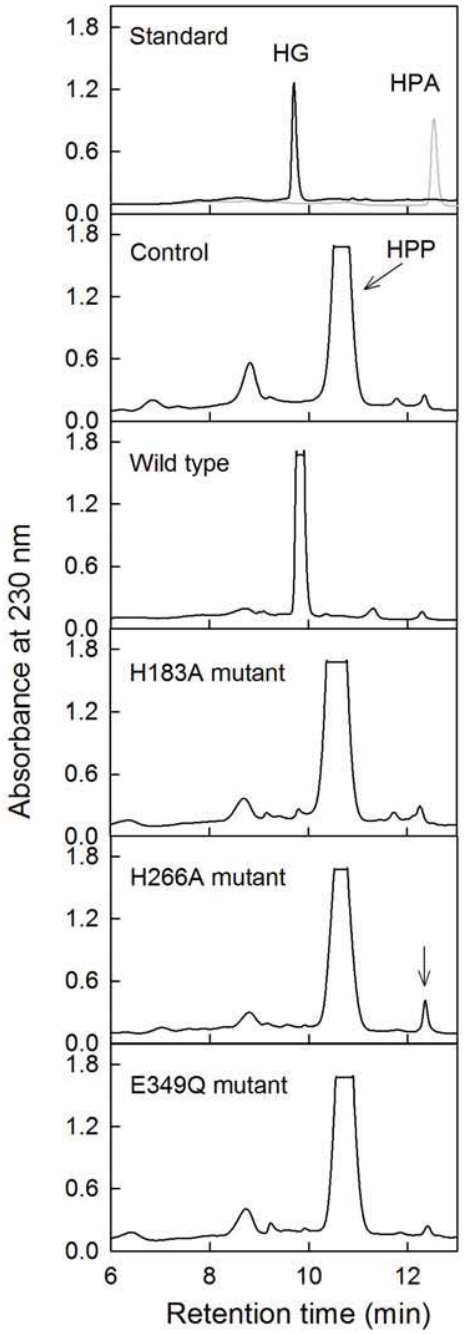

CW Huang et al., Fig. 3

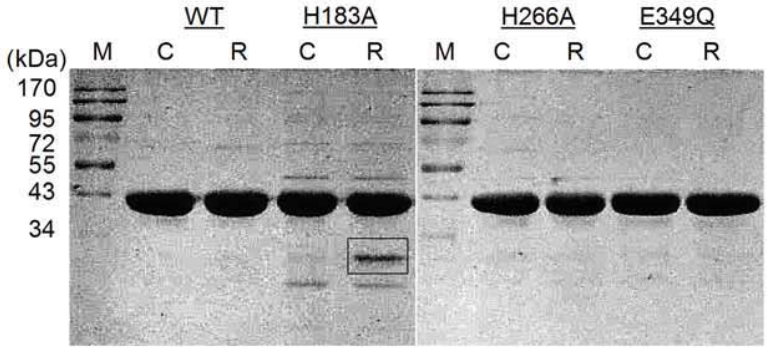

CW Chuang et al., Fig. 4

(A)

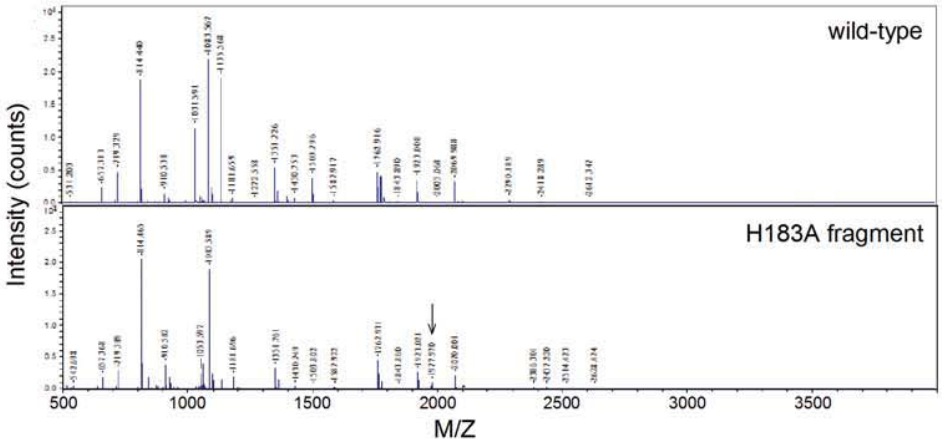

(B)

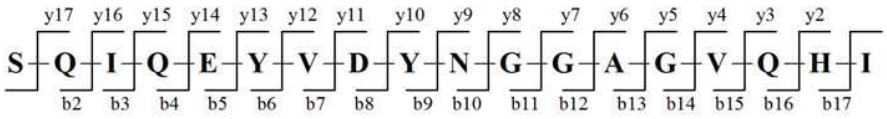

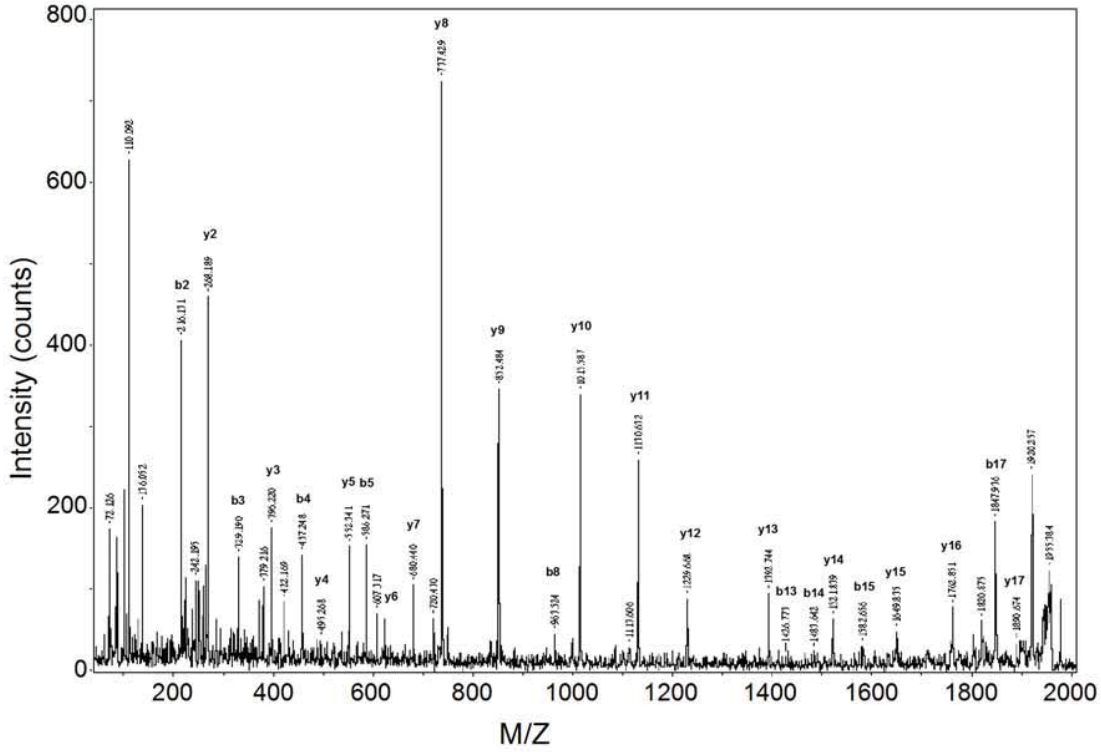

CW Huang et al., Fig. 5

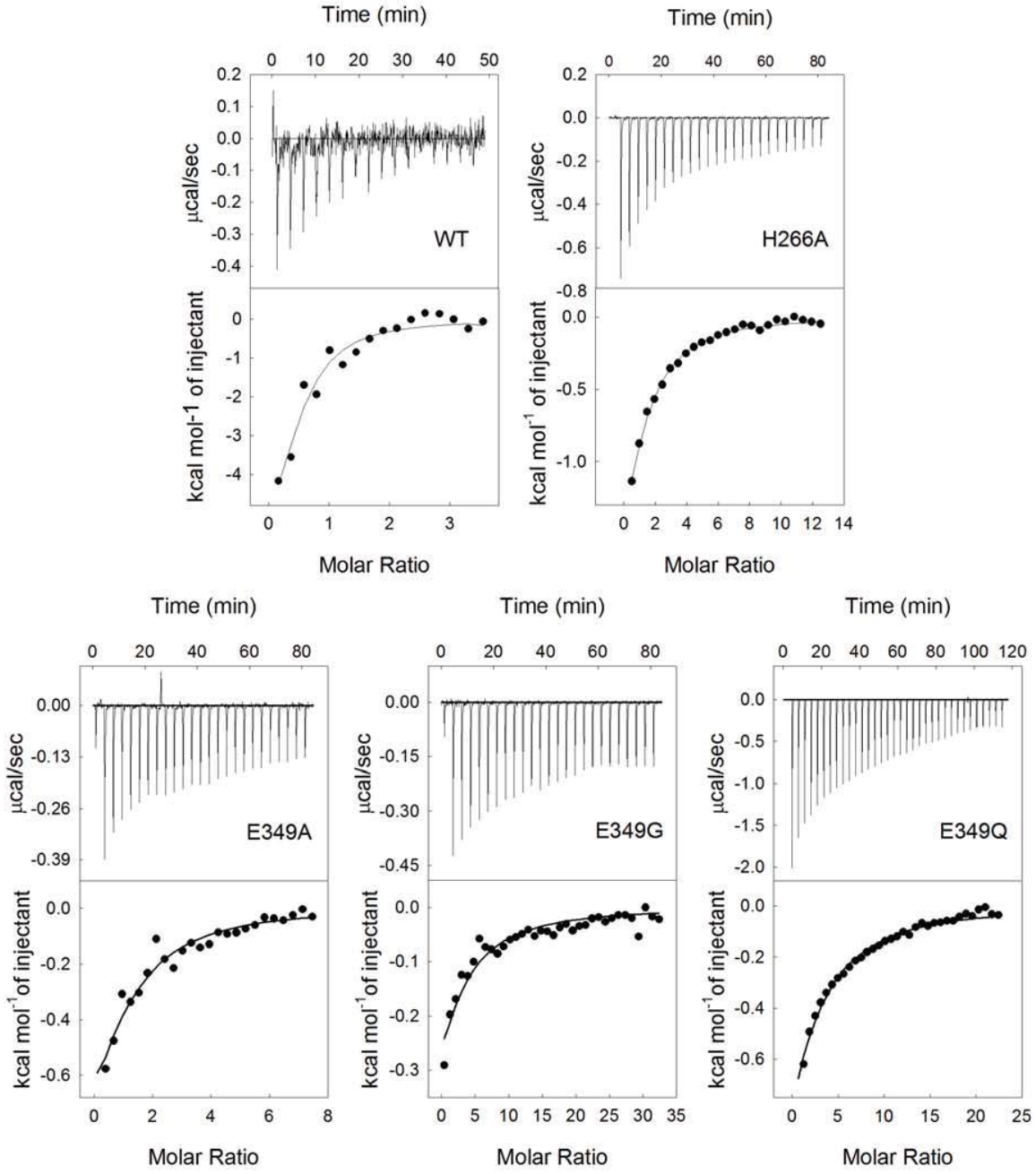

CW Huang et al. Fig. 6